scientific reports

Check for updates

OPEN

Sodium propionate protects against bronchopulmonary dysplasia by inhibiting IL-17-mediated apoptosis of alveolar epithelial cells

Anni Xie[1,4], Weilin Qian[1,4], Danni Ye[1], Xianhui Deng[2], Yizhe Ma[2], Ran Wang[1], Qin Zhou[3]✉, Zhidan Bao[2]✉ & Renqiang Yu[1]✉

Sodium propionate (SP) has been shown to enhance alveolar growth retardation in Bronchopulmonary Dysplasia (BPD), but the mechanism remains unclear. The aim of this study is to explore the potential mechanism of SP in the treatment of BPD by utilizing animal and cell models along with bioinformation analysis. Neonatal mice were exposed to either air (21% O_2) or hyperoxia (85% O_2) from the first day after birth to establish the BPD model. The neonatal mice were intraperitoneally injected with normal saline (control group) or SP (500 mg/kg, SP group) from day 8 to day 14. SP significantly reduced the inflammatory condition of alveolar septal thickening, and decreased the alveolar fusion and mitigated weight loss in BPD mice. ELISA results demonstrated that SP significantly inhibited the secretion of IL-17, IL-6 and TNFα. Transcriptome analysis confirmed that IL-17 signaling pathway is closely related to the therapeutic effects of SP on BPD. In addition, MX2, MMP10, IL-11, ZMAT4 and SEC1 genes were identified as key and potential targets involved in the mechanism of SP treating BPD. Meanwhile, in mouse alveolar epithelial cells, apoptosis was induced by hyperoxia, but it was reduced following SP intervention. The expression of IL-17 pathway related genes: IL-17A, IL-6, TNFα and cox2 was decreased in hyperoxia treated cells after SP intervention. In conclusion, through transcriptome analysis, animal and cell experiments, we explored the role of sodium propionate in attenuating apoptosis in a BPD model through IL-17 pathway.

Keywords Bronchopulmonary dysplasia, Apoptosis, Sodium propionate, IL-17, Alveolar epithelial cells

Bronchopulmonary dysplasia (BPD) is a chronic lung disease in preterm infants. The incidence of BPD is associated with a higher risk of neonatal death[1]. BPD is associated with complex factors, including maternal chorioamnionitis during pregnancy, patent ductus arteriosus, air pollution[2], individual and genetic susceptibility, immature lung development, oxygen poisoning, mechanical ventilation lung injury, infection and inflammatory response, etc. As the rate of second births increases, so does the survival and morbidity of second births[3]. BPD also causes other diseases, such as asthma[2]. The pathogenesis of BPD is complex, including vascular development arrest, alveolar simplification, inflammation, oxidative stress and infection. While for the treatment of BPD, there is a study that showed that infants treated with ibuprofen early did not have a reduced incidence of developing moderate to severe BPD[4].

The cytokine IL-17 plays an important role in human health and diseases. When IL-17 interacts with other inflammatory factors IL-6 and IL-8, it has a strong biological activity. When the IL-17 pathway is activated during fetal growth, the fetal inflammatory response will be aggravated, and the incidence of neonatal related diseases such as BPD will be increased[5]. Elevated IL-17A expression and alveolar simplification are observed in lung inflammation induced by LPS[6]. At the same time, IL-17-driven inflammation can lead to the further

[1]Department of Neonatology, Affiliated Women's Hospital of Jiangnan University, Wuxi Maternity and Child Health Care Hospital, Wuxi 214002, China. [2]Department of Neonatology, Jiangyin People's Hospital of Nantong University, Jiangyin 214400, China. [3]Department of Pediatric, Wuxi Yihe Gynaecology and Obstetrics Hospital, Wuxi 214124, China. [4]Anni Xie and Weilin Qian contributed equally to this work. ✉email: zhouqin0546@163.com; baodandancandy@126.com; yurenqiang553@163.com

development of pulmonary inflammation, such as chronic obstructive pulmonary disease, lung cancer, pulmonary fibrosis and asthma[7]. The lung is exposed to a large number of foreign microorganisms, and IL-17A plays an important role in the clearance of pathogens[8]. However, IL-17 is also involved in inflammatory cell exudation and airway remodeling in chronic respiratory diseases[9]. These are important and complex processes.

KEGG is a database resource that integrates various biological objects and has a variety of classifications[10]. In the KEGG IL-17 Pathway (Pathway map04657), IL-17 signaling pathway consists of IL-17A-F cytokines and plays a crucial role in both acute and chronic inflammatory responses[11–13]. IL-17A plays an important role in the drive of psoriasis[14,15], causing airway inflammation and airway remodeling in asthma patients[16]. But the IL-17A signaling axis is not all negative for health[17]. For example, IL-17F plays a major role in mucosal defense[18]. IL-17 and other cytokines have unique pathophysiological effects. The IL-17 family signals through its corresponding receptors to activate downstream pathways, including NF-κB, MAPKs, and C/ebp, inducing the expression of antimicrobial peptides, cytokines, and chemokines. The effect of IL-17 on apoptosis is complex. Some studies have shown that IL-17 can inhibit tumor cell apoptosis[19–21]. However, other studies have shown that IL-17 induces apoptosis[22–24], these cells are usually those of normal tissue, such as endothelial cells[23] and lung epithelial cells[24]. According to a study, S100A9, a key biomarker, aggravated LPS-induced lung injury and apoptosis in mouse epithelial cells through IL-17-NFκB-caspase-3 signaling pathway[25]. Moreover, KEGG Pathway map04657 showed that epithelial cells treated with IL-17A, IL-17E and IL-17F showed different downstream gene changes and different phenotypes. We selected one phenotype, apoptosis, to further verify the IL-17 pathway.

Oxidative stress plays an important role in the pathogenesis of BPD. Oxidative stress causes a variety of cell death in different ways, including apoptosis, autophagy and ferroptosis[26]. Neutrophil elastase is present in the airway of BPD patients, which causes airway remodeling, impaired ciliary motility, and promotes apoptosis and senescence to prevent epithelial cell repair[27]. The key cause of alveolar dysplasia in BPD is apoptosis of lung epithelial cells[28]. By targeting apoptosis and inflammation, BPD can be relieved[29]. The occurrence of BPD in neonates can cause hippocampal neuron apoptosis and cognitive impairment, and activate caspase-dependent and caspase-independent pathways[30].

Previous studies from our research group have shown that SP can reduce lung inflammation in mice through different signaling pathways[31,32]. SP is one of the short-chain fatty acids produced by intestinal flora after fermenting dietary fiber, which has anti-inflammatory and antioxidant effects[33]. It has gained more and more research value because of its satisfactory preventive and therapeutic effects. SP also inhibits apoptosis to decrease a variety of diseases[34–36]. Metabolites produced by anaerobic fermentation in the lung: short-chain fatty acids, have the ability to inhibit IL-17A[37]. And valproic acid, a short-chain fatty acid. It can reduce the apoptosis of retinal ganglion cells and the inflammation of optic nerve in the optic neuritis model rats, such as reducing the expression of IL-17[38]. The potential mechanism of its treatment for various diseases was confirmed. Recent studies have shown that SP reduces the progression of inflammation by participating in various pathological mechanisms. Based on the above pharmacological effects of SP, especially the anti-inflammatory and antioxidant capacity, this provides a theoretical basis for the treatment of BPD. It is well known that the pathogenesis of BPD is not clear, but there is no doubt that inflammation is involved in the pathogenesis of BPD. Therefore, we focused on the roles or signal transduction mechanisms of other genes and proteins in BPD pathophysiology, and hoped to explore related regulatory genes and proteins that might be exerted by SP through this study, including alveolar developmental pathways, inflammatory pathways, and the possible role of SP.

Results

Sodium propionate decreases alveolar development and weight gain in BPD mice

In order to investigate the therapeutic effects of SP on BPD, we established a BPD model using 85% O_2 exposure. HE staining of lung sections revealed a significant reduction in the number of alveoli and thickening of the alveolar septa in BPD mice. SP treatment significantly reduced the number of alveoli and inhibited the thickening of alveolar septa in BPD mice (Fig. 1A). Additionally, the radial alveolar count (RAC) in the BPD group was reduced compared to the control group, while the SP-treated group showed an increased RAC (Fig. 1B). BPD mice exhibited significant weight loss, while SP-treated BPD mice regained their body weight (Fig. 1C). These results suggest that SP has a potential therapeutic effect on improving alveolar development and promoting weight recovery in BPD mice.

Transcriptomic analysis identifies key genes regulated by sodium propionate in BPD treatment and validation of key genes in BPD mice

To explore the molecular mechanisms by which SP alleviates BPD, we conducted transcriptomic sequencing of lung tissue from BPD mice. Principal component analysis (PCA) of gene expression in BPD mice and in the control group, revealed significant differences between the two groups (Fig. 2A). Which is the same between BPD mice and SP group (Fig. 2B).We identified 2299 differentially expressed protein-coding genes among control group and BPD group, with 931 upregulated and 1368 downregulated genes, when log2 fold changes were ≥ 1 or ≤ -1. The threshold to log2 fold changes of ≥ 1 and ≤ -1 among BPD group and SP group. Under these conditions, 345 differentially expressed genes were identified, with 283 upregulated and 62 downregulated genes. Volcano plot and heatmap were utilized to show the expression patterns of DEGs in this dataset (Fig. 2C–F). The results of the GO analysis showed in Fig. 2G, H. These findings suggest that SP modulates the expression of key genes that may contribute to its therapeutic effects on BPD. Machine learning was performed on the differentially expressed genes of these three sets of data: LASSO and Support Vector machine with Recursive Feature Elimination (SVM-RFE). Although several key genes were found, the confidence was not high due to the small sample size. Therefore, genes were selected for verification according to the methods used in the literature[39].To validate the transcriptomic data, we performed RT-PCR on right lung tissue from BPD and SP-treated BPD mice. We compared the differentially expressed genes (DEGs) between the BPD and control

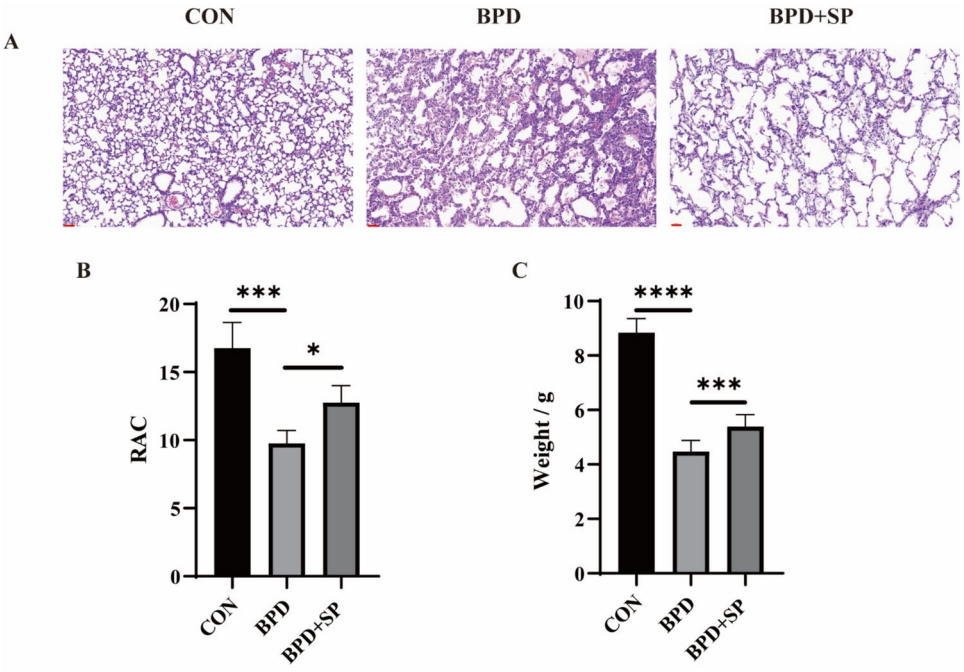

Fig. 1. Alleviation of BPD with SP. **A** HE staining showed that the alveolar space was thickened and the alveolar space was reduced in BPD mice, which was reversed by SP intervention. Scale bars, 50 μm, n = 6/group. **B** The lung RAC of BPD mice decreased, and the reduction of RAC was increased in the SP treatment group. **C** BPD mice lost weight, and mice treated with SP gained weight.

groups, and between the BPD and SP treatment groups. Our results showed that MX2, MMP10, and IL-11 were upregulated in the BPD and control groups, and downregulated following SP treatment (Fig. 2I). Additionally, ZMAT4 and SEC1 were downregulated in the BPD and control groups but were significantly upregulated in the SP treatment group. These results confirm that SP treatment regulates the expression of key genes involved in BPD pathogenesis, as validated by RT-PCR.

KEGG pathway analysis reveals IL-17 pathway involvement in SP treatment of BPD and ELISA analysis

To further investigate the pathways involved in SP's therapeutic effects on BPD, we performed KEGG pathway analysis on the differentially expressed genes identified in the transcriptomic sequencing. The analysis revealed that the IL-17 signaling pathway was significantly upregulated in the BPD group. However, SP treatment resulted in a marked downregulation of IL-17 pathway expression (Fig. 3A, B). These findings suggest that the IL-17 pathway plays a crucial role in the pathogenesis of BPD and that SP may exert its therapeutic effects by modulating this pathway.To assess the effect of SP on inflammatory cytokine secretion, we performed ELISA analysis on plasma samples from BPD and SP-treated BPD mice. The results showed that the IL-17A secretion in the BPD group was 57.27 pg/ml, significantly higher than the 42.43 pg/ml observed in the SP-treated group (p = 0.0149). Similarly, IL-6 levels were higher in the BPD group (17.02 pg/ml) compared to the SP group (11.72 pg/ml, p = 0.0180), and TNF-α levels were also significantly elevated in the BPD group (36.31 pg/ml) compared to the SP group (4.41 pg/ml, p = 0.0091). These results indicate that SP treatment significantly reduces the secretion of inflammatory cytokines, including IL-17A, IL-6, and TNF-α, in BPD mice (Fig. 3C). Furthermore, the expression of other inflammatory factors associated with IL-17A was also upregulated in BPD and significantly decreased in the SP-treated group (Fig. 3D). These findings suggest that SP modulates the inflammatory response in BPD.

SP reduces hyperoxia-induced apoptosis in alveolar epithelial cells and mice

To evaluate the effect of SP on hyperoxia-induced apoptosis in alveolar epithelial cells, we exposed MLE-12 cells to 85% O_2 and treated them with SP in vitro. Western blot and mRNA expression analysis revealed that hyperoxia exposure increased the expression of pro-apoptotic proteins Caspase3 , Cleaved-caspase-3 and Bax, while it decreased the anti-apoptotic protein Bcl2. SP treatment reversed these effects, reducing Caspase3 and Bax expression while increasing Bcl2 expression (Fig. 4A, C, E). The expression of these apoptosis-specific genes showed the same trend in mice lung (Fig. 4B, D, F). Flow cytometry analysis showed that the proportion of late apoptotic cells was significantly higher in the hyperoxia group, but SP treatment reversed this trend, reducing apoptosis (Fig. 4G). TUNEL staining further confirmed that SP treatment significantly reduced apoptosis in alveolar epithelial cells under hyperoxic conditions (Fig. 4H–I). These results suggest that SP effectively reduces apoptosis in alveolar epithelial cells induced by hyperoxia, potentially contributing to its therapeutic effects in BPD.

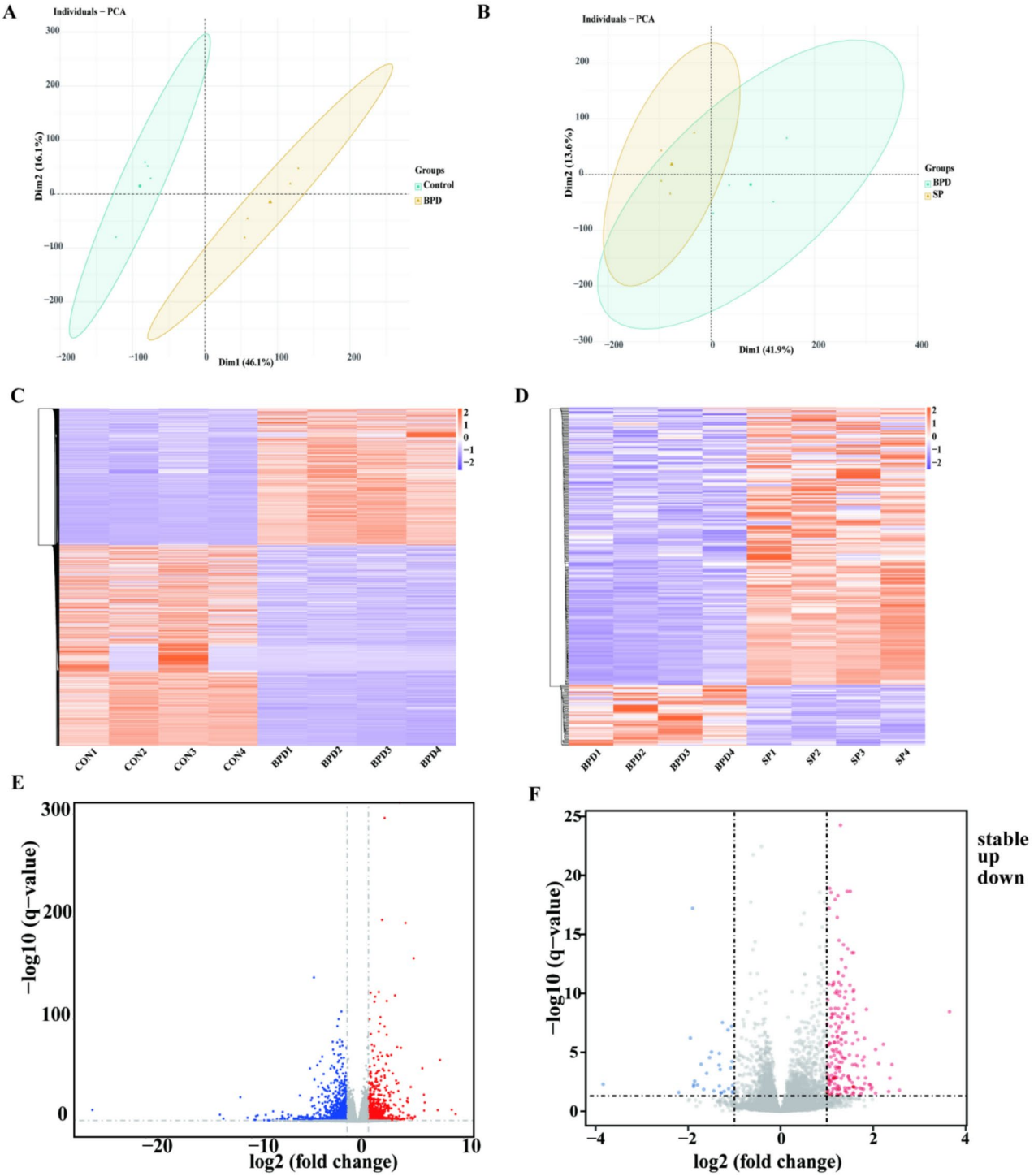

Fig. 2. The differential expression analysis of the DEGs. **A**, **B** PCA of control/BPD and BPD/SP of the lung in mice. **C**, **D**. Heat map of DEGs. **E**, **F**. The volcano map of this dataset. **G**, **H**. Gene co-expression modules of DEGs. **I** Screened for differential validation genes. Data are displayed as mean ± SEM, n = 6. * $P < 0.05$; ** $P < 0.01$; *** $P < 0.001$; **** $P < 0.0001$.

Effect of IL-17A knockdown on the intervention of sodium propionate in BPD cells model

In order to verify the effect of IL-17 pathway on apoptosis in BPD and the mechanism of SP intervention, the role of IL-17 pathway was examined. Knockdown of IL-17A was performed in a cell model. Firstly, the knockdown efficiency of SiRNA was tested, and it was found that the knockdown efficiency could reach 63% (Fig. 5A, B). Then, the expression levels of BAX, Caspase3 and Cleaved-Caspase3 in the hyperoxia treated cells were lower than those in the hyperoxia treated cells. In the cells with SP knockdown, apoptosis was reduced after hyperoxia

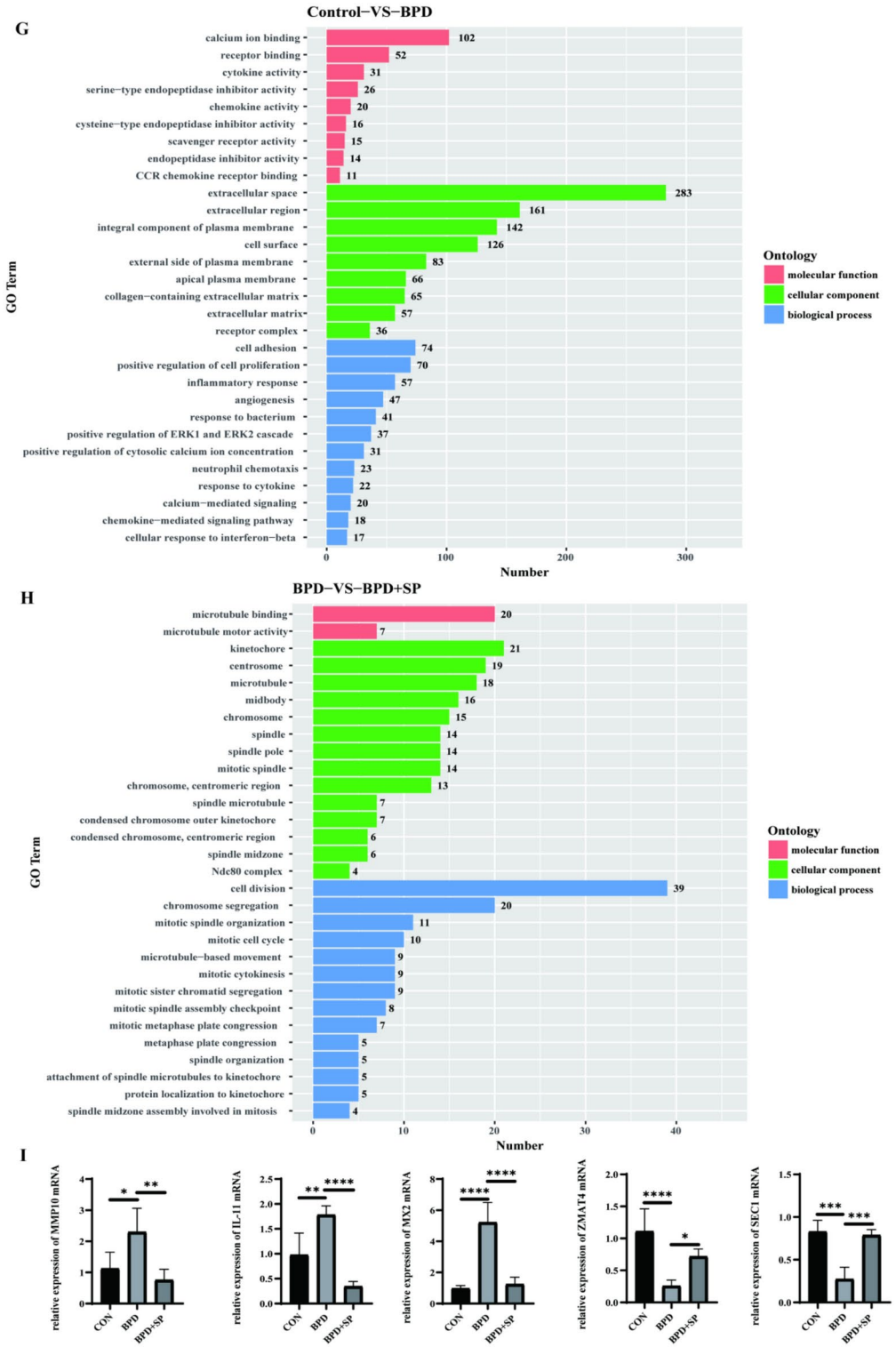

Figure 2. (continued)

treatment (Fig. 5C–F). Molecular docking was then performed to identify the binding sites of propionate on IL-17. Van der Waals forces, Coulomb forces, hydrogen bonding and hydrophobic effects were evaluated. There were three docking sites between SP and IL-17. The molecular docking 3D structure map (Fig. 6A, B) showed that SP was "wrapped" in the 3D structure of IL-17, and such a structure greatly increased the possibility of SP binding to IL-17.

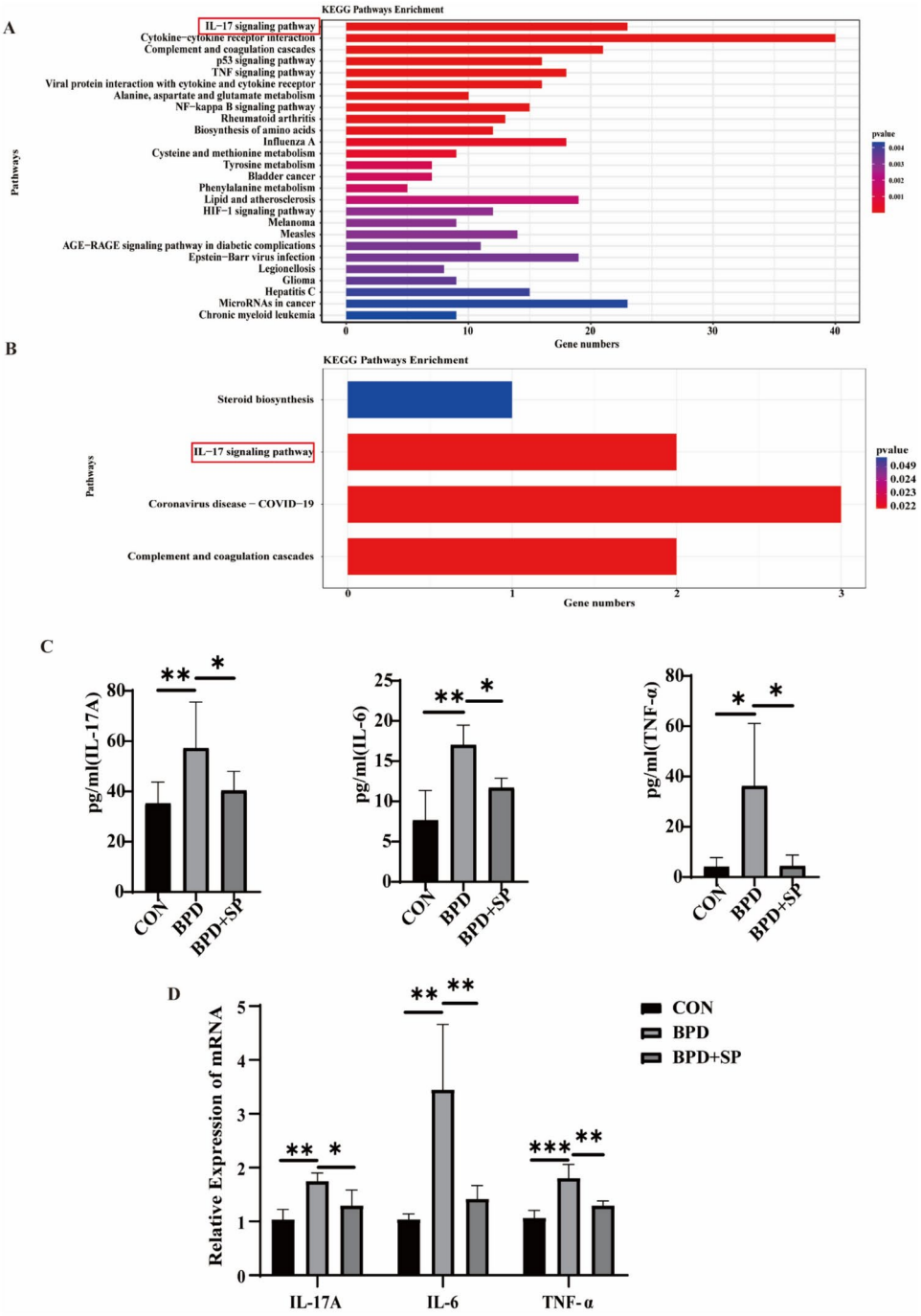

Fig. 3. **A** KEGG pathway analysis of Control group and BPD group. **B** KEGG pathway analysis of Control group and BPD group. In the red box is specific expression KEGG pathways: IL-17 pathway). **C** Verification of the IL-17 pathway. The expressions of IL-17A and IL-6 and TNF-α in serum. **D** mRNA expression of IL-17A, IL-6 and TNF-α. Data are displayed as mean ± SEM, n = 6. * $P < 0.05$; ** $P < 0.01$; *** $P < 0.001$. The KEGG analysis from (www.kegg.jp/kegg/kegg1.html).

Discussion

Alveolar septal thickening and alveolar simplification are important pathophysiological factors associated with impaired angiogenesis, oxidative stress, and inflammation in BPD. It is characterized by a decrease in the number of alveoli, enlargement and rupture of alveoli, and inflammatory factors in lung tissue are important features in BPD. Inflammation triggers the thickening of the lung septum in BPD lung tissue, hindering alveolar and intrapulmonary vascular development[40]. Inflammation in BPD comes not only from excessive or prolonged mechanical ventilation, but also from prenatal intrauterine inflammation[41]. Excessive inflammation affects lung ventilation and vascular remodeling, and this effect induces hypoxia and excessive respiratory movement[42].

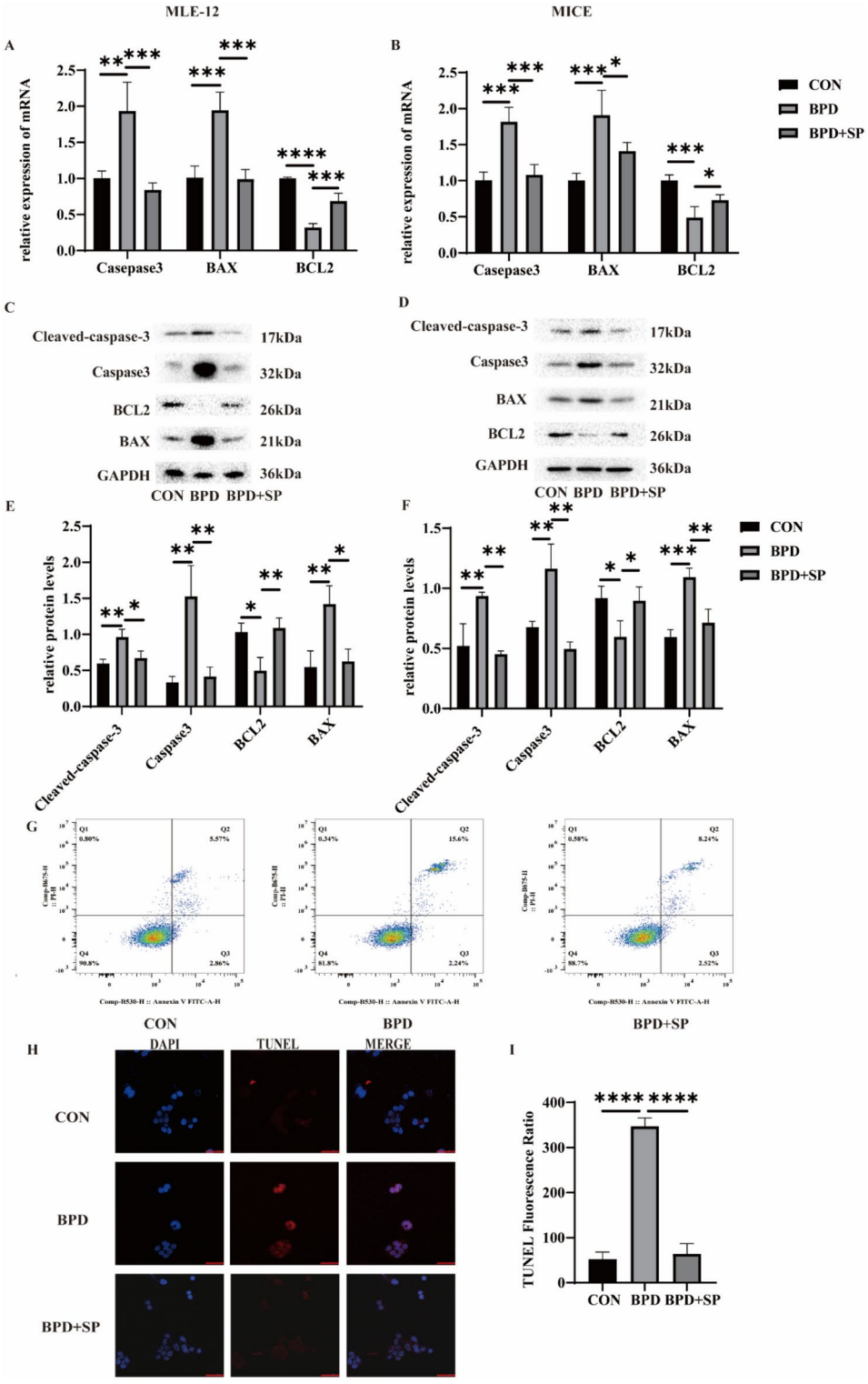

Fig. 4. Apoptosis detection of MLE-12 BPD model in vitro and lung tissue of mice. **A** In MLE-12, the mRNA expression of Casepase3 and BAX were increased in BPD groups, the mRNA expression of BCL2 were decreased in BPD groups. These trends were reversed after the intervention of SP. (n = 6.) **B** The mRNA trends in lung tissues were as same as those in MLE-12. (n = 6.) **C**, **E** In MLE-12, compared with the control group, the expressions of Caspase3, Cleaved-caspase-3 and BAX were increased and the expression of BCL2 was decreased in the hyperoxia group, and this trend was reversed after SP intervention. (n = 3). **D**, **F**. The protein expression trends in lung tissues were as same as those in MLE-12. (n = 3). **G**, **H**. Apoptosis detection of MLE-12 cells, including flow cytometry and TUNEL staining. Scale bars, 50 μm. (n = 6.) Data are displayed as mean ± SEM. $^{*}P < 0.05$; $^{**}P < 0.01$; $^{***}P < 0.001$, $^{****}P < 0.0001$.

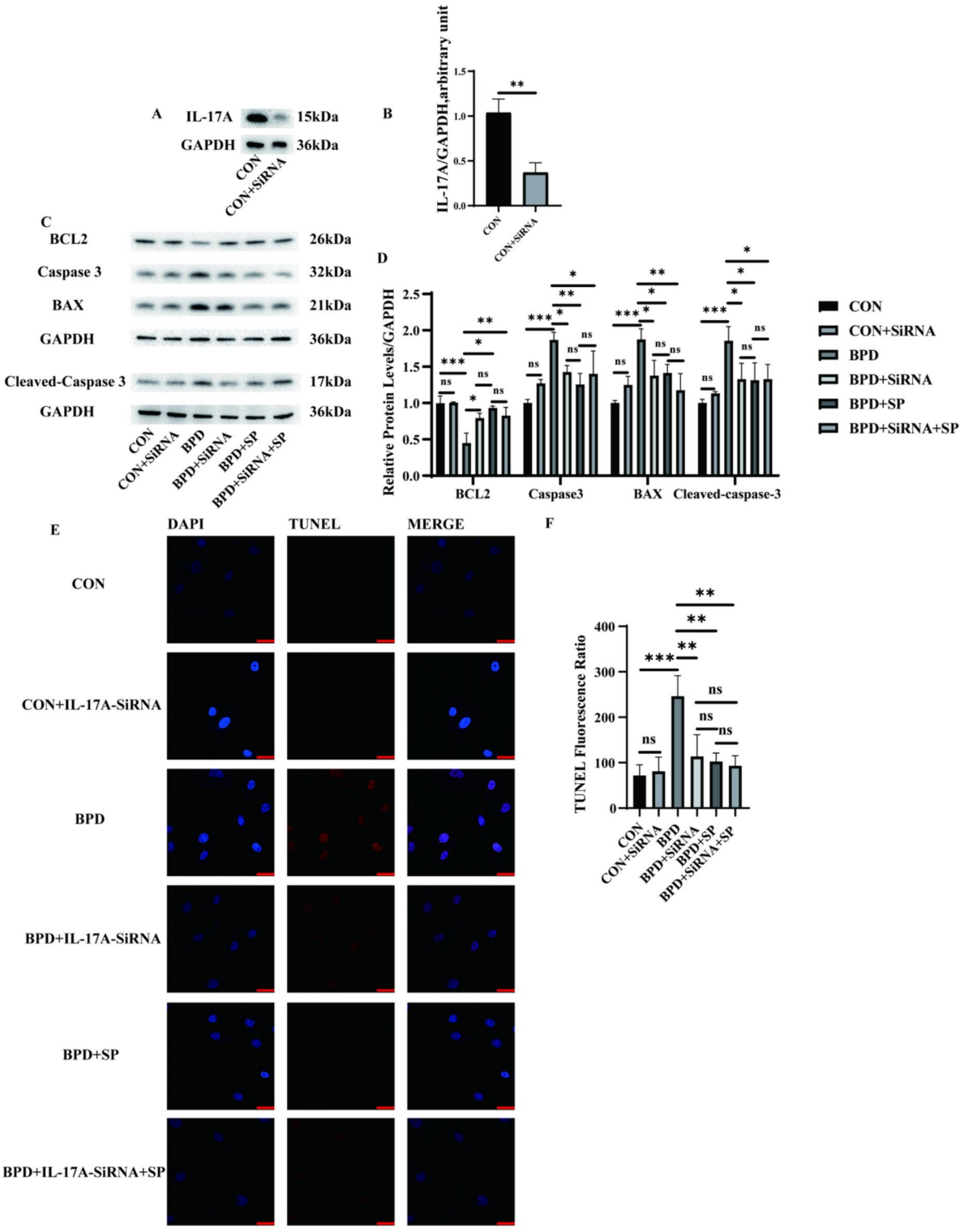

Fig. 5. Effect of IL-17A knockout on the inhibition of apoptosis in BPD cell model by SP. **A**, **B**. Verification of knockdown efficiency. **C**, **D**. Western blot analysis of apoptosis after knockdown. (n = 3) **E**, **F** Apoptosis detection of MLE-12 cells, including flow cytometry and TUNEL staining. Scale bars, 50 μm. (n = 6.) Data are displayed as mean ± SEM. * $P < 0.05$; ** $P < 0.01$; *** $P < 0.001$, ns: no significance.

Premature birth will interrupt the alveolar development of the newborn, and the number of alveoli will be smaller and the alveoli will be larger, causing a decrease in lung capacity. Although the symptoms of BPD will be relieved after the corrected gestational age, and many BPD patients can breathe normally as the alveoli continue to develop after birth, some adults with a history of BPD will have sequelae of BPD, and they are more likely to

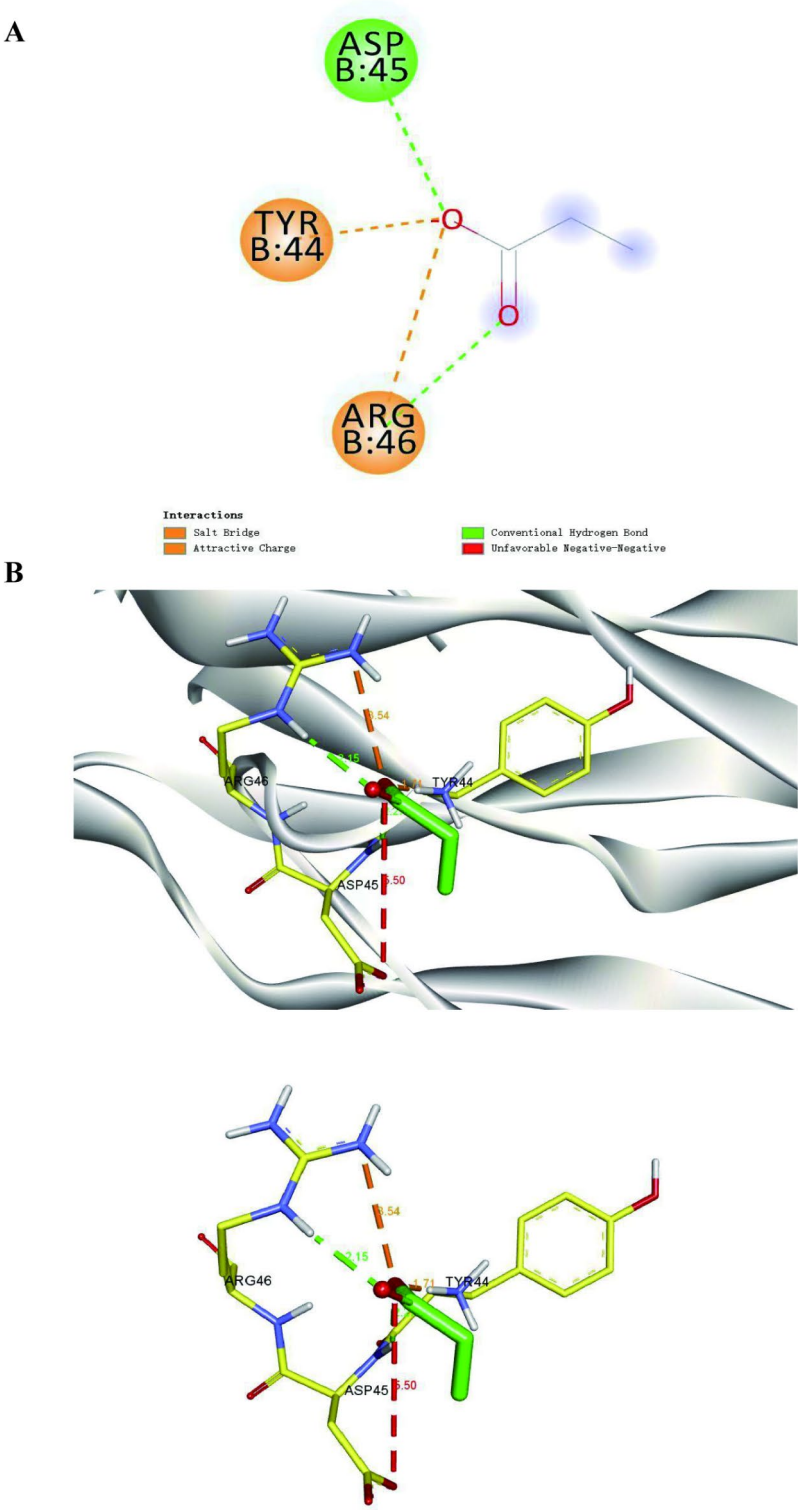

Fig. 6. Molecular docking prediction. **A** Molecular docking 2D of SP with IL-17 protein. **B** Locally magnified 3D structure of SP interacting with IL-17 protein.

develop airway obstruction and other symptoms of lung airflow obstruction[43]. Moreover, the effects of preterm birth on the lungs persist for decades, including impairment of small airway function[44,45]. Therefore, how to reverse or inhibit alveolar simplification and septal thickening is of great interest.

IL-6, IL-17A, TNF-α, and COX-2 were upregulated in the BPD group compared with the control group and downregulated in the SP treatment group compared with the BPD group. Inflammation-related signaling pathway is the classical signaling pathway of BPD, and inflammation is the main pathological mechanism of

BPD. After treatment of infected mouse macrophages with SP, the intracellular viral replication process was inhibited, and the expression of TNF-α and IL-6 was decreased[46]. In addition, SP has been reported to act by inhibiting NFκB[33] to play an anti-inflammatory role.

In addition to inflammation, oxidative stress is also an important cause of BPD. In the epigenetic and transcriptomic analysis of BPD mouse models, there were differences in the expression of genes related to oxidative stress[47]. After treatment with sodium butyrate and SP, the expression of antioxidant genes in human hepatoma cells induced by lipopolysaccharide was significantly increased[48]. It also reduced the expression of TNF-α. In addition, reactive oxygen species (ROS) -mediated oxidative stress can cause autophagy and apoptosis of cells. The relationship between apoptosis and autophagy is complex and interacts with each other at multiple levels[49]. At the same time, SP exerts anti-apoptotic effect on islet cells mediated by free fatty acid receptor 2[50]. The presence of apoptosis in BPD is evident and has been confirmed by studies[28]. However, in the present study, through transcriptome sequencing, it was found that SP ameliorated apoptosis through Th-17 pathway and ameliorated the symptoms of BPD mice. BCL2, an anti-apoptotic gene, was down-regulated in BPD compared with the control group and up-regulated in the SP treatment group compared with BPD. The expression of pro-apoptotic genes BAX and Caspase3 in BPD was increased, and this trend was reversed by SP.

Matrix metalloproteinases (MMPs) are zinc-dependent endopeptidases. Different MMPS exist in different compartments of cells. Matrix Metallopeptidase 10 (Mmp10) is a response gene involved in immune response. The expression of mmp10 can be promoted by IL-4 to cause macrophage polarization[51]. In mouse models of Huntington's disease[52] and ischemic model of human brain neurons after stroke[53], the expression of MMP-10 was up-regulated in both groups. In a cell experiment, knockdown of MMP-10 in cells treated with ethanol significantly increased cell survival and reduced inflammatory response[54]. Endothelial cells treated with MMP-10 knockdown significantly alleviated capillary degeneration[55], Impaired vascular development is also one of the pathogenesis of BPD. In asthmatic airway epithelial cells, the expression of MMP-10 is increased[56].

Myxovirus resistance (MX) proteins play a key role in the innate immune response to viral infection. Within several years, multiple groups have shown that human human myxovirus resistance 2 (MX2) is an interferon (IFN) -stimulating gene (ISG) with potent anti-human immunodeficiency virus 1 (HIV-1) activity[57–59], and the ability to resist hepatitis B virus replication[60]. MX2 is also a biomarker of various diseases, including systemic lupus erythematosus[61], Clear cell carcinoma of kidney[62]. Human lung epithelial cells treated with Aspergillus fumigatus Conidia and subjected to RNA sequencing showed increased expression of MX2, a gene involved in interferon signaling[63].

IL-11 is a member of the IL-6 family. There have been a lot of studies on IL-6, but there are still a lot of studies on IL-11. In silica-induced pulmonary fibrosis mice, IL-11 activates the extracellular signal-regulated kinase pathway, and knockdown of IL-11 can attenuate the effect of silica-induced pulmonary fibrosis[64]. At the same time, inhibition of IL-11 in the treatment of pulmonary fibrosis. In a study of lung tissue from BPD mice, transcriptome analysis showed increased IL-11 expression, while knockdown of IL-11 on MLE also ameliorated the effects of cells after hyperoxia stimulation[65], This is also consistent with the results of the present study.

Zinc Finger Matrin-Type 4 (ZMAT4) is a member of the zinc finger family and has a significant relationship with myopia[66], However, there are few studies on this gene.

Secretory blood group 1 (SEC1) According to a study on the molecular mechanism of inflammatory bowel disease, knockdown of SEC1 in mouse colon cancer cell line CT26 enhanced cellular immune responses and increased expression of inflammatory cytokines IL-1β, IL-6 and TNFα. At the same time, the increase of SEC1 expression can promote the increase of the number of colonic epithelial cells, reduce cell apoptosis, and repair inflammation[67]. In addition, the gut microbiota of SEC1 knockout mice was also disrupted[68]. Lung tissue sequencing results of BPD mice showed decreased expression of SEC1 relative to the control group, and this trend was reversed after intervention with SP, which was confirmed by both experimental and high-throughput sequencing.

The cytokine IL-17 plays an important role in human health and diseases. IL-17 can act synergistically with other inflammatory factors. When the IL-17 pathway is activated during fetal growth, the fetal inflammatory response will be aggravated and neonatal-related diseases such as BPD will be increased[5]. Increased IL-17A expression and alveolar simplification occur in LPS-induced lung inflammation[6], and blocking the IL-17A pathway can inhibit cell apoptosis and alleviate BPD symptoms[69]. The downstream exploration of IL-17A found that breast milk-derived exosomes reduced cell apoptosis and improved hyperoxia-induced alveolar type 2 epithelial cell damage by inhibiting the downstream FADD pathway of IL-17[70]. Knockdown of IL-17A in the cell model showed that the apoptosis was reduced after hyperoxia treatment. Molecular docking of SP and IL-17 was performed, and it was found that there was indeed a binding site.

However, our study only focused on one pathway and phenotype of IL-17 pathway, and there are many other pathways and mechanisms to be explored. However, another study showed that the Universidade Federal do Parana collected lung tissue samples from 32 neonates from 1991 to 2005. After immunohistochemistry analysis, it was found that IL-17A expression was increased in the non-BPD group, compared with the BPD group. The researchers suggest that IL-17A may be a protective factor for BPD[71]. In a study involving 125 neonates, salivary IL-17 levels were significantly lower in BPD group than in control group[72].

In addition, there may be more than one pathway by which SP alleviates BPD symptoms. SP can induce apoptosis of breast cancer cells through JAK2-STAT3-ROS-p38 MAPK pathway and inhibit tumor growth[73]. SP can also inhibit harmful inflammatory responses, inhibit apoptosis, and protect the blood-milk barrier through the NF-κB pathway[34]. In colon cancer, SP reduces the expression of protein arginine methyltransferase 1 through the mTOR pathway and induces apoptosis of cancer cells[74]. In conclusion, IL-17 is not the only pathway affected by SP, but further pathway exploration was not carried out in this paper. This will be further investigated in the upcoming experiments conducted by of our research group.

The pathogenesis of BPD is associated with inflammation, obstructed alveolar development, and impaired vascular development. SP showed a significant protective effect on reversing alveolar simplification and inhibiting inflammatory response. The therapeutic effect of SP on BPD may be attributed to its effect on IL-17 signaling pathway, and SP inhibited apoptosis and reduced inflammatory response in the MLE-12 hyperoxia model. In addition, MMP10, MX2, IL-11, ZMAT4, and SEC1 are key genes related to the mechanism of action of SP on BPD; however, the specific mechanism of the action of SP in the treatment of BPD needs to be further verified.

Methods

Treatment of animals

C57BL/6J mice were ordered from SLAC ANIMAL (Shanghai, China). The methods used to create animal models refer to previous literature[75]. Newborn C57BL/6J mice were randomly divided into a model group, a control group and a SP-treated group after their natural birth. In the model group and SP-treated group, the inhaled oxygen concentration was 85%O_2. After seven days, the SP-treated group were injected SP until 14 days. The mice in the control group inhaled air (FiO_2 21%). The hyperoxia chamber we used had an oxygen concentration sensor that showed the oxygen concentration in the chamber in real time to be 85%O_2. The hyperoxic chamber has a fan to maintain temperature and humidity, and the temperature inside the chamber is displayed in real time. At the same time, the temperature and humidity in the animal laboratory were kept constant. Temperatures ranged from 20°C to 26°C and humidity was maintained between 40% and 70%. SP (SP, Sangon, Shanghai, China) was dissolved in PBS and administered subcutaneously at a dose of 500 mg/kg once a day for seven consecutive days. This dose was selected based on previous studies[76]. Mother mice in the model group and the control group were exchanged daily to eliminate feeding differences and avoid oxygen poisoning. All mice were sacrificed at the end of day 14, the anesthesia was given with 1.5% isoflurane. All animal study procedures were approved by the Ethics Committee for Animal Care and Use of Jiangnan University (Approval No. JN. No 20240315c0180630[108]). All methods were conducted according to relevant guidelines and regulations which are reported under the ARRIVE guidelines[77].

Transcriptome sequencing and gene expression analysis

RNA sequencing (RNA-Seq) and analysis were performed by AZENTA company (SuZhou, China). 1 μg total RNA was used for following library preparation. The poly(A) mRNA isolation was performed using Oligo(dT) beads. The mRNA fragmentation was performed using divalent cations and high temperature. Priming was performed using Random Primers. First strand cDNA and the second-strand cDNA were synthesized. The purified double-stranded cDNA was then treated to repair both ends and add a dA-tailing in one reaction, followed by a T-A ligation to add adaptors to both ends. Size selection of Adaptor-ligated DNA was then performed using DNA Clean Beads. Each sample was then amplified by PCR using P5 and P7 primers and the PCR products were validated. Then libraries with different indexes were multiplexed and loaded on an Illumina HiSeq/ Illumina Novaseq/ MGI2000 instrument for sequencing using a 2x150 paired-end (PE) configuration according to manufacturer's instructions. In order to remove technical sequences, including adapters, polymerase chain reaction (PCR) primers, or fragments thereof, and quality of bases lower than 20, pass filter data of fastq format were processed by Cutadapt (V1.9.1, phred cutoff: 20, error rate: 0.1, adapter overlap: 1bp, min. length: 75, proportion of N: 0.1) to be high quality clean data. Firstly, reference genome sequences and gene model annotation files of relative species were downloaded from genome website, such as UCSC, NCBI, ENSEMBL. Secondly, Hisat2 (v2.2.1) was used to index reference genome sequence. Finally, clean data were aligned to reference genome via software Hisat2 (v2.2.1). Expression analysis in the beginning transcripts in fasta format are converted from known gff annotation file and indexed properly. Then, with the file as a reference gene file, HTSeq (v0.6.1) estimated gene and isoform expression levels from the pair-end clean data. The fragments per kilobase per million mapped reads (FPKM) was utilized to calculate gene expression. The DESeq2 R software (version 1.42.0 https://github.com/thelovelab/DESeq2). was applied to evaluate the DEGs. In order to reduce the false discovery rate, the obtained p-values were modified using Benjamini and Hochberg's method. The differential expression of mRNA was analyzed using the limma package in R software (version 4.2.2). Genes meeting the criteria of adjusted P-values <0.05, absolute log2 fold changes > 1 and < -1 were classified as DEGs. Gene Ontology (GO) annotation analysis was conducted using the "cluster Profiler" R package (version 4.10.0) in this article. A significance threshold of P-value < 0.05 was established to identify statistically significant results in the analysis. In this study, Kyoto Encyclopedia of Genes and Genomes (KEGG) Annotation Analysis (www.kegg.jp/kegg/kegg1.html) was conducted using the "cluster Profiler" R package. A statistical significance threshold of P-value < 0.05 was proved to distinguish significant results in the analysis.

Quantitative real-time PCR (RT-PCR) analysis

Specific genes that were differentially expressed in control and BPD groups and BPD and SP treatment groups were identified using RT-PCR. In addition, we validated the expression of other inflammatory factors (IL-17A, IL-6, and TNF-α) associated with the expression of IL-17A (interleukin-17A) and lung damage proteins. Right lung tissue from mice was isolated and total RNA was extracted using trizol (Cwbio, China). Reverse transcription was carried out using the PrimeScript RT reagent Kits. RT-PCR was conducted using quantitative PCR with SYBR Premix Ex Taq TM (Vazyme, Nanjing, China). The expressions of mRNA were quantified employing the comparative cycle threshold (Ct) method, where the relative quantification of target transcript levels was determined by subtracting Ct values of target genes from Ct values of GAPDH. To compare the differences between different groups. The results for each gene were measured from at least three independent replicates (n = 6/ group). Primers of related genes are shown in Table 1.

Gene	Sequences (5'–3')
Casepase3	F: AAGATACCGGTGGAGGCTGA
	R: AAGGGACTGGATGAACCACG
BCL2	F: ATGTGTGTGGAGAGCGTCAAC
	R: AGACAGCCAGGAGAAATCAAAC
BAX	F: AGACAGGGGCCTTTTTGCTA
	R: AATTCGCCGGAGACACTCG
IL-17A	F: ACAGTGAAGGCAGCGGTACT
	R: GCTCAGAGTCCAGGGTGAAG
IL-6	F: CAAAGCCAGAGTCCTTCAGAG
	R: AGCATTGGAAATTGGGGTAG
TNF-α	F: CCCTCACACTCAGATCATCTTCT
	R: GCTACGACGTGGGCTACAG
MX2	F: ACACGGTCACTGAAATTGTACG
	R: TGGAGTCGGATTGACATCTCTG
MMP10	F: GAGCCACTAGCCATCCTGG
	R: CTGAGCAAGATCCATGCTTGG
IL-11	F: TGCTGACAAGGCTTCGAGTAG
	R: ACATCAAGAGCTGTAAACGGC
ZMAT4	F: AGCCTGGTTTAACAATCCTCTG
	R: AGCTGCTCTAGCAAGGCAAC
SEC1	F: CACTGGCCCGGATGAATGG
	R: GTATCCTGTGAAGCGCACATAG
GAPDH	F: CTGGAAAGCTGTGGCGTGAT
	R: GACGGACACATTGGGGGTAG

Table 1. Primer sequences.

Histological tests

The mice lung tissues were removed and placed in 4% paraformaldehyde, which was then given to YIERMEI Bio (Nanjing, China), making paraffin sections and HE staining.

Enzyme-linked immunosorbent assay (ELISA)

In this transcriptome sequencing, the IL-17 pathway was the SP effect pathway for treating BPD, while IL-17A was the upstream molecule of this pathway. Many studies demonstrated that IL-17A stimulates the release of pro-inflammatory cytokines (IL-6 and TNF-α), which participate in the inflammatory mechanism of BPD. The samples of plasma were analyzed using ELISA kits (Fine Biotech, Wuhan, China). The results for each plasma sample originated from three independent repeated measurements (n = 6 / group).

Cell cultivation

Mouse alveolar epithelial cells (MLE-12) were cultured in DMEM containing 10% FBS, 100 U/ml penicillin, and 100 μg/ml streptomycin, at 37 °C in 85% O_2 and 5% CO_2. Cultured MLE-12 cells were subjected to hyperoxia induction and SP treatment. To conduct the hyperoxia experiments, we used subconfluent cells (at 70% with approximately 350–400 cells/mm^2) and placed them in sealed glass chambers filled with a gas mixture of 85% O_2 and 5% CO_2. The cells were then incubated at 37 °C for 48 h. To serve as a control, cells were maintained under normal air conditions, of 21% O_2 and 5% CO_2 at 37 °C. To examine the effect of SP on MLE-12 cells under hyperoxia conditions, the cells were grouped into the Control group, Hyperoxia group, and Hyperoxia+SP group. The Control group was maintained in normal air. The Hyperoxia group was exposed to hyperoxia, while the Hyperoxia+SP group was pretreated with SP 2h before exposure to hyperoxia. SP (0.6mM) was dissolved in DMEM. SP was procured from Sangon (Shanghai, China). In this study, the expression of IL-17A gene in MLE-12 cells was interfered by transient transfection of small interfering RNA. The sequence of IL-17A-siRNA was purchased from KGI Biotech (Jiangsu), and the interference and control sequences were IL-17A-siRNA: No.WR24051705603:5 '-CCUGUCACUAUUUGGAGCUUUTT-3'; RX0102035:5 '-GCAAGGGCAUCCUGG GAAATT-3'. MLE-12 cells were seeded in 12-well plates at a density of 3×10^4 cells/cm^2, and when the cell density reached 80%, transfection experiments were performed. Two 1.5 mL centrifuge tubes were prepared in an ultra-clean platform, and 250 μL basal medium was added to each tube.5μmol siRNA was added to the siRNA tube according to the proportion, and the mixture was gently blown by a pipetting machine. In the transfection reagent tube, 5 μL of LipofectamineTM 3000 transfection reagent was added in proportion, and the mixture was gently blown with a pipetting gun. Then the liquid in the configured transfection reagent tube was added into the siRNA tube according to the ratio, and gently blew again to be uniform. The cells were incubated at room temperature for 5 min to fully bind. Then the incubated siRNA mixture was evenly added into the corresponding wells, gently shaken and mixed, and placed in the cell incubator at 37 ℃. Four hours after transfection, the

corresponding drug addition and hyperoxia treatment were carried out for 24 hours. After completion of the treatment, total cell protein was extracted for subsequent experiments.

Western blot

The levels of IL-17A, Cleaved-caspase-3, caspase3, Bcl2, Bax, and GADPH were assessed through Western blotting. The protein concentration was determined by BCA method. Subsequently, the proteins (30 μg) were separated via 10% SDS-PAGE and transferred onto PVDF membranes. The membranes were blocked with 5% skimmed milk powder for 2.5h, then incubated with primary antibodies (1:1000) overnight at 4 °C for 12h, followed by incubation with secondary antibodies (1:5000) for 1h. Band visualization was conducted using a Tanon 5200 imager. Each experiment was conducted in triplicate. The Cleaved-caspase-3 antibody was procured from CST (Cell Signaling Technology, American). The caspase3, Bcl2, Bax and IL-17A antibodies were procured from MedChemExpress (Shanghai, China), while the GAPDH antibody was acquired from ProteinTech (Wuhan, China).

Apoptosis analysis

Cell apoptosis was analyzed with an Annexin V–fluorescein isothiocyanate apoptosis detection kit (Elabscience, Wuhan, China). The cells were digested by trypsin without EDTA for 90 s. Both attached and nonattached cells were harvested and stained with fluorescein isothiocyanate–conjugated Annexin V and propidium iodide and then analyzed by flow Jo. Alveolar epithelial cell apoptosis was expressed as a percentage of Annexin V–positive cells to total cells. The TUNEL (Elabscience, Wuhan, China) dyeing process of cells is carried out in accordance with the reagent company instructions and is examined using confocal microscopy.

Molecular docking prediction

According to the Chemical Abstracts Service (CAS) number of small molecules, the 3D structure in SDF format was obtained from PubChem database, and the structure was imported into ChemBio3D Ultra14.0 for energy minimization. The Minimum RMS Gradient was set to 0.001 and the small molecules were saved in mol2 format. The optimized small molecules were imported into AutodockTools-1.5.6 for hydrogenation, charge calculation, charge distribution and rotatable bond setting, and then saved as "pdbqt" lattice formula. Sodium propionate (SP) was downloaded from the protein Structure bank (PDB), and Pymol2.3.0 software was used to remove protein crystal water and original ligand, etc. The protein structure was imported into AutoDocktools (v1.5.6) for hydrogenating, calculating charge, assigning charge and specifying atom type and saved as "pdbqt" format. The POCASA1.1 online tool (https://g6altair.sci.hokudai.ac.jp/g6/services/pocasa/) was used to predict the protein binding sites, and AutoDock Vina1.1.2 software was used for molecular docking. PyMOL2.3.0 software was used to analyze the interaction mode of the docking results.

Statistical analysis

GraphPad Prism 9.0 was used to generate all graphs and conduct statistical analyses. Datas were subjected to one-way ANOVA. Data are presented as means ± standard deviation. When a p value of less than 0.05, it indicates a significant difference between groups. Adobe Illustrator 2024 was used for data analysis and image processing.

Data availability

The datasets used and analysed during the current study available from the corresponding author on reasonable request.

Received: 18 November 2024; Accepted: 17 March 2025
Published online: 05 April 2025

References

1. Dassios, T. et al. Mortality after 36 weeks postmenstrual age of extremely preterm infants in neonatal care: The impact of growth impairment and bronchopulmonary dysplasia. *Early Hum Dev* **171**, 105618 (2022).
2. Kelchtermans, J. et al. Ambient air pollution and outpatient morbidities in bronchopulmonary dysplasia. *Ann Am Thorac Soc* **21**(1), 88–93 (2024).
3. Del Pino Hernández, I. L. et al. Birth order and morbidity and mortality to hospital discharge among inborn very low-birthweight, very preterm twin infants admitted to neonatal intensive care: a retrospective cohort study. *Arch Dis Child Fetal Neonatal Ed* **108**(4), 354–359 (2023).
4. Gupta, S. et al. Trial of selective early treatment of patent ductus arteriosus with ibuprofen. *N Engl J Med* **390**(4), 314–325 (2024).
5. Lawrence, S. M., Ruoss, J. L. & Wynn, J. L. IL-17 in neonatal health and disease. *Am J Reprod Immunol* **79**(5), e12800 (2018).
6. Cui, T. X. et al. IL-17a-producing γδT cells and NKG2D signaling mediate bacterial endotoxin-induced neonatal lung injury: Implications for bronchopulmonary dysplasia. *Front Immunol* **14**, 1156842 (2023).
7. Ritzmann, F., et al., *IL-17 Cytokines and Chronic Lung Diseases.* Cells, 2022. **11**(14).
8. Gurczynski, S. J. & Moore, B. B. IL-17 in the lung: the good, the bad, and the ugly. *Am J Physiol Lung Cell Mol Physiol* **314**(1), L6-l16 (2018).
9. Tan, H. L. & Rosenthal, M. IL-17 in lung disease: friend or foe?. *Thorax* **68**(8), 788–790 (2013).
10. Kanehisa, M. et al. KEGG for taxonomy-based analysis of pathways and genomes. *Nucleic Acids Res* **51**(D1), D587-d592 (2023).
11. Miossec, P. & Kolls, J. K. Targeting IL-17 and TH17 cells in chronic inflammation. *Nat Rev Drug Discov* **11**(10), 763–776 (2012).
12. Kim, T.S., et al. Neutrophil extracellular traps and extracellular histones potentiate IL-17 inflammation in periodontitis. *J. Exp. Med.* 2023. **220**(9).
13. Li, X. et al. IL-17 receptor-based signaling and implications for disease. *Nat Immunol* **20**(12), 1594–1602 (2019).
14. Tan, H. B., Zheng, Y. Q. & Zhuang, Y. P. IL-17A in diabetic kidney disease: protection or damage. *Int Immunopharmacol* **108**, 108707 (2022).
15. Fischer, B. et al. IL-17A-driven psoriasis is critically dependent on IL-36 signaling. *Front Immunol* **14**, 1256133 (2023).

16. Quan, J. et al. Epithelial SIRT6 governs IL-17A pathogenicity and drives allergic airway inflammation and remodeling. *Nat Commun* **14**(1), 8525 (2023).
17. Lorè, N. I., Bragonzi, A. & Cigana, C. The IL-17A/IL-17RA axis in pulmonary defence and immunopathology. *Cytokine Growth Factor Rev* **30**, 19–27 (2016).
18. Iwakura, Y. et al. Functional specialization of interleukin-17 family members. *Immunity* **34**(2), 149–162 (2011).
19. Li, J. et al. IL-17 promotes hepatocellular carcinoma through inhibiting apoptosis induced by IFN-γ. *Biochem Biophys Res Commun* **522**(2), 525–531 (2020).
20. Song, Y. et al. IL-17 affects the progression, metastasis, and recurrence of laryngeal cancer via the inhibition of apoptosis through activation of the PI3K/AKT/FAS/FASL pathways. *J Immunol Res* **2020**, 2953191 (2020).
21. Picard, F. S. R. et al. IL-17A-producing CD8(+) T cells promote PDAC via induction of inflammatory cancer-associated fibroblasts. *Gut* **72**(8), 1510–1522 (2023).
22. Paira, D. A. et al. Interferon γ, IL-17, and IL-1β impair sperm motility and viability and induce sperm apoptosis. *Cytokine* **152**, 155834 (2022).
23. Zhu, F. et al. IL-17 induces apoptosis of vascular endothelial cells: A potential mechanism for human acute coronary syndrome. *Clin Immunol* **141**(2), 152–160 (2011).
24. Bai, S. et al. IL-17 stimulates neutrophils to release S100A8/A9 to promote lung epithelial cell apoptosis in Mycoplasma pneumoniae-induced pneumonia in children. *Biomed Pharmacother* **143**, 112184 (2021).
25. Pei, H. et al. S100A9 exacerbates sepsis-induced acute lung injury via the IL17-NFκB-caspase-3 signaling pathway. *Biochem Biophys Res Commun* **710**, 149832 (2024).
26. Deng, X. et al. Molecular mechanisms of cell death in bronchopulmonary dysplasia. *Apoptosis* **28**(1–2), 39–54 (2023).
27. Voynow, J. A. and Shinbashi, M. Neutrophil elastase and chronic lung disease. *Biomolecules*, 2021. **11**(8).
28. Tong, X., et al. Hyperoxia induces endoplasmic reticulum stress-associated apoptosis via the IRE1α pathway in rats with bronchopulmonary dysplasia. *Mol. Med. Rep.*, 2021; **23**(1).
29. Hu, J. et al. Vitamin D ameliorates apoptosis and inflammation by targeting the mitochondrial and MEK1/2-ERK1/2 pathways in hyperoxia-induced bronchopulmonary dysplasia. *J Inflamm Res* **15**, 4891–4906 (2022).
30. Yin, R. et al. Neonatal bronchopulmonary dysplasia increases neuronal apoptosis in the hippocampus through the HIF-1α and p53 pathways. *Respir Physiol Neurobiol* **220**, 81–87 (2016).
31. Chen, D. et al. Sodium propionate attenuates the lipopolysaccharide-induced epithelial-mesenchymal transition via the PI3K/Akt/mTOR signaling pathway. *J Agric Food Chem* **68**(24), 6554–6563 (2020).
32. Chen, D. et al. Sodium propionate enhances Nrf2-mediated protective defense against oxidative stress and inflammation in lipopolysaccharide-induced neonatal mice. *J Inflamm Res* **14**, 803–816 (2021).
33. Filippone, A., et al. The Anti-inflammatory and antioxidant effects of sodium propionate. *Int. J. Mol. Sci.*, 2020; **21**(8).
34. Ali, I. et al. Sodium propionate protect the blood-milk barrier integrity, relieve lipopolysaccharide-induced inflammatory injury and cells apoptosis. *Life Sci* **270**, 119138 (2021).
35. Kim, K. et al. Propionate of a microbiota metabolite induces cell apoptosis and cell cycle arrest in lung cancer. *Mol Med Rep* **20**(2), 1569–1574 (2019).
36. Li, W. F. et al. Combination of sodium butyrate and decitabine promotes transgene expression in CHO cells via apoptosis inhibition. *N Biotechnol* **69**, 8–17 (2022).
37. Segal, L. N. et al. Anaerobic bacterial fermentation products increase tuberculosis risk in antiretroviral-drug-treated HIV patients. *Cell Host Microbe* **21**(4), 530-537.e4 (2017).
38. Liu, Q. et al. Valproic acid attenuates inflammation of optic nerve and apoptosis of retinal ganglion cells in a rat model of optic neuritis. *Biomed Pharmacother* **96**, 1363–1370 (2017).
39. Yue, H. et al. Curcumin, novel application in reversing myocardial fibrosis in the treatment for atrial fibrillation from the perspective of transcriptomics in rat model. *Biomed Pharmacother* **146**, 112522 (2022).
40. Wang, S. H., Tsao, P. N. Phenotypes of bronchopulmonary dysplasia. *Int. J. Mol. Sci.* 2020; **21**(17).
41. Yu, H. et al. Fetal origin of bronchopulmonary dysplasia: contribution of intrauterine inflammation. *Mol Med* **30**(1), 135 (2024).
42. Collaco, J. M. & McGrath-Morrow, S. A. Respiratory phenotypes for preterm infants, children, and adults: bronchopulmonary dysplasia and more. *Ann Am Thorac Soc* **15**(5), 530–538 (2018).
43. Landry, J. S., *et al*. Lung function and bronchial hyperresponsiveness in adults born prematurely. A cohort study. *Ann. Am. Thorac. Soc.* 2016. **13**(1), 17–24.
44. Walicka-Serzysko, K. et al. Long-term pulmonary outcomes of young adults born prematurely: A Polish prospective cohort study PREMATURITAS 20. *BMC Pulm Med* **24**(1), 126 (2024).
45. Lundberg, B., et al. Lung function in young adulthood in relation to moderate-to-late preterm birth. ERJ Open Res. 2024. **10**(1).
46. Kim, H., et al., *The Modulatory Effect of Sodium Propionate Treatment in the Expression of Inflammatory Cytokines and Intracellular Growth of Brucella abortus 544 in Raw 264.7 Cells.* J Microbiol Biotechnol, 2023. **33**(8): p. 1006–1012.
47. Kimble, A., Robbins, M. E., Perez, M. Pathogenesis of bronchopulmonary dysplasia: Role of oxidative stress from 'omics' studies. *Antioxidants (Basel)*, 2022; **11**(12).
48. Cook, K. J. et al. Sodium propionate or sodium butyrate promotes fatty acid oxidation in HepG2 cells under oxidative stress. *J Med Food* **26**(1), 74–79 (2023).
49. Sharma, P. et al. Oxidative stress-induced apoptosis and autophagy: Balancing the contrary forces in spermatogenesis. *Biochim Biophys Acta Mol Basis Dis* **1869**(6), 166742 (2023).
50. Pingitore, A. et al. Short chain fatty acids stimulate insulin secretion and reduce apoptosis in mouse and human islets in vitro: Role of free fatty acid receptor 2. *Diabetes Obes Metab* **21**(2), 330–339 (2019).
51. Chang, L. et al. MMP10 alleviates non-alcoholic steatohepatitis by regulating macrophage M2 polarization. *Int Immunopharmacol* **124**(Pt B), 111045 (2023).
52. Miller, J. P. et al. Matrix metalloproteinases are modifiers of huntingtin proteolysis and toxicity in Huntington's disease. *Neuron* **67**(2), 199–212 (2010).
53. Cuadrado, E. et al. Vascular MMP-9/TIMP-2 and neuronal MMP-10 up-regulation in human brain after stroke: A combined laser microdissection and protein array study. *J Proteome Res* **8**(6), 3191–3197 (2009).
54. Chang, Y. et al. Gentiopicroside ameliorates ethanol-induced gastritis via regulating MMP-10 and pERK1/2 signaling. *Int Immunopharmacol* **90**, 107213 (2021).
55. Saunders, W. B., Bayless, K. J. & Davis, G. E. MMP-1 activation by serine proteases and MMP-10 induces human capillary tubular network collapse and regression in 3D collagen matrices. *J Cell Sci* **118**(Pt 10), 2325–2340 (2005).
56. Kuo, C. S. et al. Contribution of airway eosinophils in airway wall remodeling in asthma: Role of MMP-10 and MET. *Allergy* **74**(6), 1102–1112 (2019).
57. Betancor, G. et al. MX2-mediated innate immunity against HIV-1 is regulated by serine phosphorylation. *Nat Microbiol* **6**(8), 1031–1042 (2021).
58. Guo, H., et al. The SAMHD1-MX2 axis restricts HIV-1 infection at postviral DNA synthesis. *mBio*, 2024. **15**(7), e0136324.
59. Layish, B. et al. Virus specificity and nucleoporin requirements for MX2 activity are affected by GTPase function and capsid-CypA interactions. *PLoS Pathog* **20**(3), e1011830 (2024).
60. Wang, Y. X. et al. Interferon-inducible MX2 is a host restriction factor of hepatitis B virus replication. *J Hepatol* **72**(5), 865–876 (2020).

61. Meng, X. W. et al. MX2: Identification and systematic mechanistic analysis of a novel immune-related biomarker for systemic lupus erythematosus. *Front Immunol* **13**, 978851 (2022).
62. Wei, Y. et al. Identification of MX2 as a novel prognostic biomarker for sunitinib resistance in clear cell renal cell carcinoma. *Front Genet* **12**, 680369 (2021).
63. Kushima, H., et al. Effects of aspergillus fumigatus conidia on apoptosis and proliferation in an in vitro model of the lung microenvironment. *Microorganisms*, 2021; **9**(7).
64. Xie, Y. et al. Interleukin-11 drives fibroblast metabolic reprogramming in crystalline silica-induced lung fibrosis. *Sci Total Environ* **949**, 174976 (2024).
65. Zhu, H., et al. Interleukin-11 is involved in hyperoxia-induced bronchopulmonary dysplasia in newborn mice by mediating epithelium-fibroblast cross-talk. *Inflammation*, 2024.
66. Cheong, K. X. et al. Association of VIPR2 and ZMAT4 with high myopia. *Ophthalmic Genet* **41**(1), 41–48 (2020).
67. Cai, J. et al. Sec1 regulates intestinal mucosal immunity in a mouse model of inflammatory bowel disease. *BMC Immunol* **24**(1), 51 (2023).
68. Ren, Z., et al. Expression analysis and the roles of the Sec1 gene in regulating the composition of mouse gut microbiota. Genes (Basel), 2022; **13**(10).
69. Goates, M. et al. Blocking IL-17a signaling decreases lung inflammation and improves alveolarization in experimental bronchopulmonary dysplasia. *Am J Pathol* **194**(11), 2023–2035 (2024).
70. Zhou, Y. et al. Human breast milk-derived exosomes through inhibiting AT II cell apoptosis to prevent bronchopulmonary dysplasia in rat lung. *J Cell Mol Med* **26**(15), 4169–4182 (2022).
71. Witkowski, S. M. et al. Analysis of interleukins 6, 8, 10 and 17 in the lungs of premature neonates with bronchopulmonary dysplasia. *Cytokine* **131**, 155118 (2020).
72. Su, T. Y. et al. Salivary cytokine - A non-invasive predictor for bronchopulmonary dysplasia in premature neonates. *Cytokine* **148**, 155616 (2021).
73. Park, H. S. et al. Sodium propionate exerts anticancer effect in mice bearing breast cancer cell xenograft by regulating JAK2/STAT3/ROS/p38 MAPK signaling. *Acta Pharmacol Sin* **42**(8), 1311–1323 (2021).
74. Ryu, T. Y. et al. Downregulation of PRMT1, a histone arginine methyltransferase, by sodium propionate induces cell apoptosis in colon cancer. *Oncol Rep* **41**(3), 1691–1699 (2019).
75. Nardiello, C. et al. Standardisation of oxygen exposure in the development of mouse models for bronchopulmonary dysplasia. *Dis Model Mech* **10**(2), 185–196 (2017).
76. Choi, J. et al. Pathophysiological and neurobehavioral characteristics of a propionic acid-mediated autism-like rat model. *PLoS ONE* **13**(2), e0192925 (2018).
77. Percie du Sert, N., et al. The ARRIVE guidelines 2.0: Updated guidelines for reporting animal research. *PLoS Biol*., 2020; **18**(7): e3000410.

Acknowledgements

This work was supported by National Natural Science Foundation of China (No. 82101812), Jiangsu Commission of Health and Family Planning (No. Z2020042), the Wuxi Commission of Health and Family Planning (No. M202414), the Wuxi Association for Science and Technology (Nos. KX-23-C022 and KX-24-C258), and Jiangyin Young and Middle-aged Talent Program (No. JYROYT202304).

Author contributions

AX: Writing–original draft, Experimental measurements, Data analysis. WQ: Writing–original draft. DY: Experimental measurements. XD: Data analysis. YM: Experimental measurements. RW: Visualization. ZB: Writing–review & editing. QZ: Experimental measurements, Methodology, Conceptualization. RY: Writing–review and editing, Funding acquisition, Resources, Methodology, Conceptualization.

Declarations

Competing interests

The authors declare no competing interests.

Additional information

Supplementary Information The online version contains supplementary material available at https://doi.org/10.1038/s41598-025-94794-5.

Correspondence and requests for materials should be addressed to Q.Z., Z.B. or R.Y.